

International Workshop on Computational Nanotechnology

P:05 Characterization of topological phase transitions in silicene and other 2D gapped Dirac materials

J C Bolívar Fernández¹, F de los Santos¹, J B Roldán² and E Romera¹

¹Instituto Carlos I de Física Teórica y Computacional, Spain, ²Departamento de Electrónica y Tecnología de Computadores, Spain

In this work, we have studied the time evolution of electron wave packets in a monolayer of silicene under perpendicular magnetic and electric fields to characterize the topological band insulator transitions. We have found that the periodicities exhibited by the wave packets dynamics (zitterbewegung, classical and revival times) reach maximum values at the charge neutrality points (CNP). Additionally, we have discovered that electron currents reflect the transitions from a topological insulator to a band insulator at CNP too. These results are valid for other 2D gapped Dirac materials analogous to silicene with a buckled honeycomb structure and a significant spin-orbit coupling [1-4].

- [1] E. Romera, J. C. Bolívar, J. B. Roldán and F. de los Santos, Revivals of electron currents and topological-band insulator transitions in 2D gapped Dirac materials, EPL, 115, 20008 (2016).
- [2] M. Calixto and E. Romera, Inverse participation ratio and localization in topological insulator phase transitions, Journal of Statistical Mechanics, P06029 (2015).
- [3] E. Romera and M. Calixto. Uncertainty relations and topological-band insulator transitions in 2D gapped Dirac materials. Journal of Physics: Condensed Matter, 27, 175003 (2015).
- [4] M. Calixto and E. Romera. Identifying topological-band insulator transitions in silicene and other 2D gapped Dirac materials by means of Rényi-Wehrl entropy. EPL, 109, 40003 (2015).

P:06 study of ballistic transport in phosphorene--nanoribbon-- FETs using empirical pseudopotentials

S Chen¹, J Fang², W G Vandenberghe¹, and M V Fischetti¹

¹The University of Texas at Dallas, USA, ²Vanderbilt University, USA

Among the 2D materials currently being considered as possible channel materials for future field-effect transistors, mono- and multi-layer phosphorous (phosphorene) stands out for its promising fabrication and electron-transport properties: Experimental FETs have shown a high on-off current ratio and with a field-effect carrier mobility of the order of 10^3 cm²/Vs in few-layer phosphorene [1]. Here we present an empirical-pseudopotential study of ballistic quantum transport in monolayer phosphorene in order to assess its potential application in nanoelectronics, following the methodology we have developed before [2].

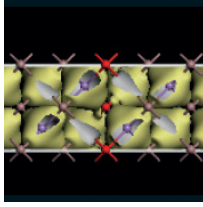
BAND STRUCTURE CALCULATION AND TRANSPORT SIMULATION

Monolayer phosphorene exhibits a band gap of 1.5 eV [3]. In order to reproduce correctly this experimental observation, we have considered a previously proposed functional form for the local empirical pseudopotential phosphorous [4],

$$V_P(q) = \sum_{j=0}^4 a_j e^{-b_j(q-c_j)^2} [1 - d_j e^{-f_j q^2}]$$

and calibrated it obtaining the band structure shown in Fig. 1. The pseudopotential for the H required to terminate the P dangling bonds was taken from Ref. 5 without modifications:

$$V_H(q) = \begin{cases} b_0 + b_1 q + b_2 q^2 + b_3 q^3 & \text{for } (q \leq 2) \\ b_{-1}/q + b_{-2}/q^2 + b_{-3}/q^3 + b_{-4}/q^4 & \text{for } (q > 2) \end{cases}$$



International Workshop on Computational Nanotechnology

The parameters are listed in Table 2. Looking at Fig. 1, compared to results obtained using density functional theory (DFT) [6], we obtain a similar dispersion but with the desired larger band gap of 1.5 eV for infinite sheets of monolayer phosphorene. Moving to the phosphorene nanoribbons (PNRs) of interest, we show in Fig. 2 the atomic configuration of a PNR with armchair edges and a width of 16 atomic lines (16-aPNR). The band structure of an unpassivated and an H-passivated 16-aPNR is shown in Fig. 3. The passivated 16-aPNR, which has no dangling bonds band after passivation, has a band gap of 1.36 eV.

We have simulated n-FETs based on such nanoribbons using the methodology presented in Ref. [2]. In order to limit simulation time, we have restricted our attention to a narrow ribbon, a 5-aPNR (*i.e.*, 0.664 nm-wide, with a calculated band gap of 1.92 eV) and a device with a 5.496 nm gate-length. Figure 4 shows the potential and charge density profile. Fig. 5 shows the $I_{DS} - V_{GS}$ characteristics of a 5-aPNRFET, compared to the (5×5)-SiNWFET and 7-aGNRFET we have studied in Ref. 7, while Fig. 6 shows the on-current per unit width of these three devices. The 5-aPNRFET has a satisfactory subthreshold slope of about 70 mV/decade, but not quite as good as the turn-on behavior of the n-channel Si NWs. Also, the ballistic characteristics of this phosphorene-based FET (Fig. 6) are inferior to SiNW-FETs but superior to aGNR-FETs. Moreover, a relatively low electron mobility ($\sim 170 \text{ cm}^2/\text{Vs}$ along the armchair direction [8]) is likely to limit even more their performance in realistic situations.

a _i	b _i	c _i	d _i
-1.02921	0.834517	0.0	0.04
-0.048431	3.18979	0.88964	5.00
-0.11789	0.473822	1.02836	139.2
-0.073056	5.81145	2.4098	

b _i	d _i
-0.1416	0.02898
0.000902	-0.3877
0.06231	0.9862
-0.01892	-1.022

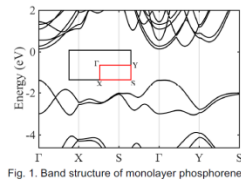


Fig. 1. Band structure of monolayer phosphorene.

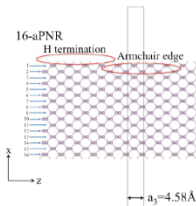


Fig. 2. Atomic model of a 16 armchair-edge phosphorene nanoribbon (16-aPNR). The electron transport direction is along z.

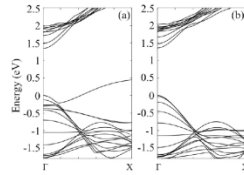


Fig. 3. Band structure of an unpassivated (a) and passivated (b) 16-aPNR.

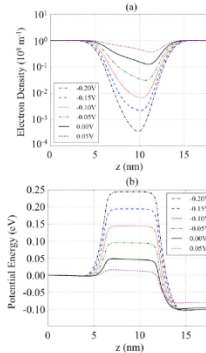


Fig. 4. Average charge-density (a) and potential energy (b) along the channel at $V_{DS}=0.10 \text{ V}$ and V_{GS} ranging from -0.20 V to 0.05 V .

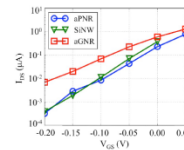


Fig. 5. $I_{DS}-V_{GS}$ characteristics of a 5-aPNRFET, (5×5)-SiNWFET (0.772 nm side-length, 5.43 nm gate-length), and 7-aGNRFET (0.739 nm-wide, 5.12 nm gate-length) at $V_{DS}=0.10 \text{ V}$. The subthreshold slope of the 5-aPNRFET is about 70 mV/dec, whereas the SiNWFETs exhibit the best electrostatic behavior.

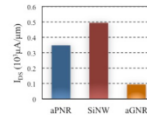
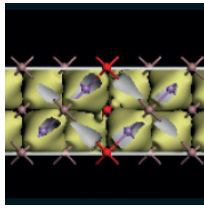


Fig. 6. I_{DS} for the 5-aPNRFET, SiNWFET, and 7-aGNRFET at $V_{DS}=0.10 \text{ V}$ and $V_{GS}-V_T=0.25 \text{ V}$. The threshold voltage (V_T) has been defined as the V_{GS} at which $I_{DS}=I_{OFF}=0.1 \mu\text{A}/\mu\text{m}$, *i.e.*, $\sim 10^{-4} I_{ON}$. The aGNRFET suffers from poor ballistic conduction.

- [1] L. Li *et al.*, Nat. Nanotech. 9, 372--377 (2012).
- [2] J. Fang, W. Vandenberghe, B. Fu, and M. V. Fischetti, J. Appl. Phys. 119, 035701 (2016).
- [3] Z. Guo *et al.*, Adv. Funct. Mater. 25, 6996 (2015).
- [4] L. Bellaiche, S.-H. Wei, and A. Zunger, Phys. Rev. B 54, 17568 (1996).



International Workshop on Computational Nanotechnology

- [5] L.-W. Wang and A. Zunger, *J. Phys. Chem.* 98, 2158 (1994).
- [6] H. Guo, N. Lu, J. Dai, X. Wu, and X. Zeng, *J. Phys. Chem. C* 118, 14051 (2014).
- [7] J. Fang, S. Chen, W. G. Vandenberghe, and M. V. Fischetti, *IEEE Trans. Elec. Dev.* (submitted, 2017).
- [8] B. Liao, J. Zhou, B. Qiu, M. Dresselhaus, and G. Chen, *Phys. Rev. B* 91, 235419 (2015).

P:07 Power dissipation and noise in spin-wave-based computing systems

G Csaba¹, Á Papp^{1,2} and W Porod²

¹Peter Pazmany Catholic University, Hungary, ²University of Notre Dame, USA

Minimizing power dissipation is one of the main drivers behind the quest for emerging electronic devices. Spin-wave-based computing and processing devices are promising candidates in this field. It is claimed that they are both fast and low-power [1][2], which are usually conflicting requirements and are difficult to achieve simultaneously in electronic (CMOS-based) computing systems.

The fact that spin-waves themselves are low-energy excitations, does not necessarily mean that computing systems built from spin-waves will be similarly low-power. There are inefficiencies in the interconversions between the electric and magnetic domains and thermal noise puts an inherent lowest limit on the energy of the spin-wave system [3]. To our knowledge, the present work is the first assessment of fundamental energy limitations in a spin-wave based computing system.

MODEL SYSTEM

The system we study is sketched in Fig 1 [2]. Electrical inputs at the left-hand side generate a spin-wave distribution in the magnetic thin film. The result of the computation is represented in the interference pattern, which should be picked up and converted back to electrical signals [3].

There are a number of physical structures that may serve as input. Most straightforwardly, the Oersted field of a waveguide may generate the spin-wavefront. More localized (short-wave) excitation can be achieved with spin-torque (for magnetic metals) or spin-orbit torque (in case of magnetic insulators) [4]. Signals can be picked up inductively, by a magnetoresistive effect or by inverse spin Hall effect (iSHE).

DISSIPATION MECHANISMS

Spin wave signals are attenuated by Gilbert damping. In metallic ferromagnets the mean free path of magnons typically up to a few ten times the wavelength of the spin wave, while in magnetic insulators it can be several hundred times their wavelength [5]. Magnetoelectric interfaces both at the input and output side yield to large insertion losses. We estimate that in the case of spin-orbit torque, 5% of the electrical input signal is converted into magnetic energy, the rest is dissipated as Joule heating on the input structure. Similarly, a mere few percent of the spin-wave energy at the output wavefront can be picked up by the output structures.

ROLE OF NOISE

Low-energy, linear spin-waves give rise to few-ten microvolts of induced AC voltage in micron- scale inductive pick up antennas, iSHE yields DC voltages with similar magnitudes. If such signals have to be picked up with significant bandwidth, thermal noise in the antenna / pick-up structure and the amplifier will become the limiting factor in the device (see Fig 2).